

# Exchange-coupling constants, spin density map, and $Q$ dependence of the inelastic neutron scattering intensity in single-molecule magnets

O. Waldmann,<sup>1,\*</sup> R. Bircher,<sup>1</sup> G. Carver,<sup>1</sup> A. Sieber,<sup>1</sup> H. U. Güdel,<sup>1</sup> and H. Mutka<sup>2</sup>

<sup>1</sup>*Department of Chemistry and Biochemistry, University of Bern, CH-3012 Bern, Switzerland*

<sup>2</sup>*Institut Laue-Langevin, 6 rue Jules Horowitz, BP 156, 38042 Grenoble Cedex 9, France*

(Dated: March 6, 2017)

The  $Q$  dependence of the inelastic neutron scattering (INS) intensity of transitions within the ground-state spin multiplet of single-molecule magnets (SMMs) is considered. For these transitions, the  $Q$  dependence is related to the spin density map in the ground state, which in turn is governed by the Heisenberg exchange interactions in the cluster. This provides the possibility to infer the exchange-coupling constants from the  $Q$  dependence of the INS transitions within the spin ground state. The potential of this strategy is explored for the  $M = \pm 10 \rightarrow \pm 9$  transition within the  $S = 10$  multiplet of the molecule  $\text{Mn}_{12}$  as an example. The  $Q$  dependence is calculated for powder as well as single-crystal  $\text{Mn}_{12}$  samples for various exchange-coupling situations discussed in the literature. The results are compared to literature data on a powder sample of  $\text{Mn}_{12}$  and to measurements on an oriented array of about 500 single-crystals of  $\text{Mn}_{12}$ . The calculated  $Q$  dependence exhibits significant variation with the exchange-coupling constants, in particular for a single-crystal sample, but the experimental findings did not permit an unambiguous determination. However, although challenging, suitable experiments are within the reach of today's instruments.

PACS numbers: 33.15.Kr, 71.70.-d, 75.10.Jm

## I. INTRODUCTION

An important issue in the field of molecular nanomagnets is the determination of the exchange-coupling constants between the metal centers in a cluster. In many of these molecules the exchange interactions are in fact the dominant terms in the spin Hamiltonian, and hence determine the nature of the ground state. The spin Hamiltonian may be written as

$$\hat{H} = - \sum_{i \neq j} J_{ij} \hat{\mathbf{S}}_i \cdot \hat{\mathbf{S}}_j + \hat{H}_A, \quad (1)$$

where the first term describes the Heisenberg exchange interactions in the cluster (each exchange bond shall be counted only once) and the second term the weaker anisotropic contributions (single-ion anisotropy, anisotropic and antisymmetric exchange, dipole-dipole interactions). The first term will be also denoted as  $\hat{H}_{ex}$ .

The single-molecule magnets (SMMs), such as the compound  $\text{Mn}_{12}$ -acetate (or  $\text{Mn}_{12}$  in short), represent important examples. The spectacular phenomena observed in these clusters, like the slow relaxation of the magnetization or quantum tunneling of the magnetization,<sup>1,2,3,4</sup> are intimately connected to a ground-state spin multiplet, which is characterized by a large spin  $S$  and a large anisotropy splitting of the easy-axis type. Obviously, the topography of the exchange-coupling constants  $J_{ij}$  is the key factor which controls the value of  $S$ . However, it also has a strong impact on the magnitude of the anisotropy splitting in the spin ground state. On the one hand, it determines how efficiently the microscopic anisotropy terms project onto the spin ground state,<sup>5</sup> and on the other hand, it generates higher-order anisotropy terms via a mixing of spin multiplets (this mechanism is also called  $S$  mixing).<sup>6,7,8,9</sup>

Typically, the SMMs are modeled by the giant-spin Hamiltonian, which essentially describes the whole molecule by a single spin  $S$ . The giant-spin Hamiltonian for  $\text{Mn}_{12}$ , for instance, usually reads (in zero field)

$$\hat{H}_S = D \left[ \hat{S}_z^2 - \frac{1}{3} S(S+1) \right] + B_{40} \hat{O}_4^0(S) + B_{44} \hat{O}_4^4(S), \quad (2)$$

where  $S = 10$ , and  $D = -0.057$  meV,  $B_{40} = -2.78 \times 10^{-6}$  meV, and  $B_{44} = -3.2 \times 10^{-6}$  meV.<sup>10</sup> The dominating  $D$  term splits the spin multiplet into  $\pm M$  sublevels, with the  $M = \pm S$  level lowest in energy. It gives rise to a large energy barrier between the  $M = +S$  and  $M = -S$  states and hence the slow relaxation of the magnetization at low temperatures. The  $B_{40}$  and  $B_{44}$  terms are fourth-order anisotropy terms.<sup>11</sup>

The giant-spin Hamiltonian approach is phenomenological in nature, but allows a very precise (in principle even exact) description of the energy eigenvalues of the ground-state multiplet, as well as their dependence on external parameters such as an applied magnetic field.<sup>15</sup> One just has to choose the spin terms as appropriate (the possible spin terms are restricted by time reversal and cluster symmetry). The results of basically all experiments on SMMs which focus on the spin ground state, be it magnetization, specific heat, electron-spin resonance, nuclear magnetic resonance, Mössbauer spectroscopy, or else, can be very well described within this framework.<sup>4</sup>

A notable exception is inelastic neutron scattering (INS). The INS selection rule  $\Delta M = 0, \pm 1$  permits transitions between adjacent  $M$  levels, which results in a typical picket-fence INS spectrum with the  $M = \pm S \rightarrow \pm(S-1)$  transition at highest energy transfers.<sup>16,17</sup> While the giant-spin Hamiltonian works well for the transition energies, the  $Q$  dependence of the INS intensity cannot be described at all in this approach. In fact, the giant-

spin Hamiltonian approach predicts the INS intensity to be constant as function of  $Q$ ,<sup>16,17</sup> while in reality it exhibits a typical oscillatory  $Q$  dependence due to the interference effects between the various spin centers in a cluster.<sup>18,19</sup> The  $Q$  dependence is hence a direct signature of the many-spin nature of the ground-state spin multiplet.<sup>7</sup> The ability of INS to probe the many-spin character of wavefunctions is unrivaled by other techniques.

This feature of INS suggests the following strategy to infer information on the exchange-coupling constants in a SMM. The INS intensity is governed by factors  $\exp[i\mathbf{Q}(\mathbf{R}_i - \mathbf{R}_j)]\langle n|\hat{S}_{i\alpha}|m\rangle\langle m|\hat{S}_{j\beta}|n\rangle$ , i.e., depends on the geometrical arrangement of the spin centers in the cluster and the local spin transition matrix elements ( $\mathbf{Q}$  is the momentum transfer vector,  $\mathbf{R}_i$  the position vector of the  $i$ th spin center,  $|n\rangle$  an eigenstate of the system, and  $\alpha, \beta = x, y, z$ ). The set of elements  $\langle n|\hat{S}_{i\alpha}|m\rangle$  may be called the spin transition map,<sup>7</sup> in analogy to the spin density map,  $\langle n|\hat{S}_{i\alpha}|n\rangle$ . Via the  $\mathbf{Q}$  vector in the exponential, the relative contribution of each of the local matrix elements  $\langle n|\hat{S}_{i\alpha}|m\rangle$  to the INS intensity can be modulated. This gives rise to interference factors and the characteristic  $Q$  dependence of the INS intensity. Hence, the  $Q$  dependence allows one to probe the topography of the spin transition map.

Within the space of the ground-state spin multiplet of a SMM, however, the transition matrix elements  $\langle n|\hat{S}_{i\alpha}|m\rangle$  are proportional to the diagonal matrix elements  $\langle n|\hat{S}_{i\alpha}|n\rangle$  in a first approximation, because of the Wigner-Eckart theorem:  $\langle \tau SM|\hat{S}_{i\alpha}|\tau SM'\rangle = C_\alpha^{MM'} \times \langle \tau S||\hat{S}_i||\tau S\rangle = C_\alpha^{MM'}/C_\alpha^{MM} \langle \tau SM|\hat{S}_{i\alpha}|\tau SM\rangle$ , where  $\langle \tau S||\hat{S}_i||\tau S\rangle$  is a reduced matrix element and  $C_\alpha^{MM'}$  are constants (essentially Wigner-3j symbols). In other words, the  $Q$  dependence of an INS transition within the ground-state multiplet is related to the spin density map, which in turn, as evident already from physical intuition, is determined by the exchange-coupling constants in the cluster. Hence, the  $Q$  dependence of the INS transitions between the  $\pm M$  levels of the spin ground state of a SMM should allow one to retrieve the exchange-coupling constants.

The novel concept in this approach should be noted. Usually, the coupling constants are determined by probing, either via spectroscopic techniques or thermal excitation, the energies of the higher lying spin multiplets. The method suggested here, in contrast, retrieves the information exclusively from the ground-state multiplet. This could be, e.g., an advantage in cases where the higher lying spin multiplets are not accessible to experiment for one or the other reason.

This work aims at exploring this strategy with the example of  $\text{Mn}_{12}$ . The  $Q$  dependence is calculated for various exchange-coupling topographies considered before in the literature, and compared to experiment. The two situations of a powder and a single-crystal sample of  $\text{Mn}_{12}$  are considered. In the powder case, the calculations are

compared to the experimental data of Hennion *et al.*,<sup>20</sup> for the single-crystal case data has been recorded on a quasi-single-crystal sample, which consisted of an oriented array of about 500 single crystals of  $\text{Mn}_{12}$ .

The outline of the manuscript is as follows. In the next section the relevant theoretical basics are presented. In Sec. III some exchange-coupling topographies are described and the reduced matrix elements or projection coefficients, respectively, calculated. In Sect. IV experimental details are given. Sections V and VI discuss the  $Q$  dependence of a powder and single-crystal SMM sample, respectively. Section VII finally presents a conclusion. Some supporting information is provided in the Appendix.

## II. BASICS

The differential neutron scattering cross section for spin clusters is given by<sup>21,22</sup>

$$\frac{d^2\sigma}{d\Omega d\omega} = C(Q, T) \sum_{nm} \frac{e^{-\beta E_n}}{Z(T)} I_{nm}(\mathbf{Q}) \delta\left(\omega - \frac{E_m - E_n}{\hbar}\right) \quad (2)$$

with

$$I_{nm}(\mathbf{Q}) = \sum_{ij} F_i(Q) F_j(Q) e^{i\mathbf{Q} \cdot \mathbf{R}_{ij}} \sum_{\alpha\beta} (\delta_{\alpha\beta} - \frac{Q_\alpha Q_\beta}{Q^2}) \times \langle n|\hat{S}_{i\alpha}|m\rangle\langle m|\hat{S}_{j\beta}|n\rangle. \quad (3)$$

Here,  $C(Q, T) = (\gamma e^2/m_e c^2)(k'/k) \exp[-2W(Q, T)]$  (all symbols have the usual meaning),  $\beta = 1/(k_B T)$ ,  $Z(T)$  is the partition function,  $F_i(Q)$  is the magnetic form factor of the  $i$ th spin center,  $\mathbf{Q} = \mathbf{k} - \mathbf{k}'$  is the transferred momentum, and  $\mathbf{R}_{ij} = \mathbf{R}_i - \mathbf{R}_j$  is the distance vector between spin  $i$  and  $j$ .  $|n\rangle$  denotes an eigenstate with energy  $E_n$  of the microscopic spin Hamiltonian  $\hat{H}$ . In this work,  $|n\rangle$  is one of the  $2S + 1$  states of the ground-state multiplet of a SMM. In the following, also the abbreviation  $l_\alpha = Q_\alpha/Q$  is used.

For a powder sample in zero magnetic field the INS intensity is obtained by averaging over all orientations of  $\mathbf{Q}$ , which yields<sup>19</sup>

$$I_{nm}(Q) = \sum_{ij} F_i^*(Q) F_j(Q) \left\{ \frac{2}{3} j_0(Q R_{ij}) \tilde{\mathbf{S}}_i \cdot \tilde{\mathbf{S}}_j + j_2(Q R_{ij}) \sum_q T_q^{(2)*}(\mathbf{R}_{ij}) T_q^{(2)}(\tilde{\mathbf{S}}_i \tilde{\mathbf{S}}_j) \right\}, \quad (4)$$

where  $j_k$  is the spherical Bessel function of order  $k$ ,  $T_q^{(k)}(\mathbf{v})$  is the  $q$ th component of the spherical tensor of rank  $k$  constructed from the Cartesian vector  $\mathbf{v}$ , and  $T_q^{(2)}(\tilde{\mathbf{S}}_i \tilde{\mathbf{S}}_j)$  represents the tensor product  $[T^{(1)}(\tilde{\mathbf{S}}_i) \otimes T^{(1)}(\tilde{\mathbf{S}}_j)]_q^{(2)}$ . The ordered products  $\tilde{S}_{i\alpha} \tilde{S}_{j\beta}$ , which appear in the explicit expression of  $T_q^{(2)}(\tilde{\mathbf{S}}_i \tilde{\mathbf{S}}_j)$ , stand for  $\langle n|\hat{S}_{i\alpha}|m\rangle\langle m|\hat{S}_{j\beta}|n\rangle$ . Equation (5) can be also written

more compactly as<sup>23</sup>

$$I_{nm}(Q) = \sum_{ij} \sum_{kq} f_{ij}^{kq}(Q, \mathbf{R}_{ij}) U_q^{(k)}(\tilde{\mathbf{S}}_i \tilde{\mathbf{S}}_j), \quad (6)$$

with the interference factors  $f_{ij}^{kq}(Q, \mathbf{R}_{ij})$  ( $k = 0, 2$  and  $|q| \leq k$ ) and the symmetrized spherical tensors  $U_q^{(k)}$  (which are proportional to  $\text{Re}[T_q^{(k)}]$  for  $q \geq 0$  and  $\text{Im}[T_q^{(k)}]$  for  $q < 0$ ). Explicit expressions for Eqs. (5) and (6) are given in Refs. [7] and [23], respectively.

Often it is desirable to describe the low-lying excitations of a spin cluster by an effective spin Hamiltonian  $\hat{H}$  instead of the microscopic spin Hamiltonian  $\hat{H}$ . The eigenstates of the effective spin Hamiltonian will be denoted as  $|\bar{n}\rangle$ , and the spin operators acting in the space of the effective spin Hamiltonian as  $\hat{S}_{j\beta}$  (effective spin operators). Since  $\hat{H}$  is supposed to yield the same energies as  $\hat{H}$ , a distinction between  $E_n$  and  $\bar{E}_n$  is not necessary. For a more detailed description of the relationships between effective and microscopic spin Hamiltonian see e.g. Ref. [7]. Using the effective spin Hamiltonian, the  $Q$  dependence of the INS intensity can be reproduced with a high degree of accuracy by a first-order perturbation theory approach.<sup>7,23</sup>

In the present context of a SMM, where the excitations within the ground-state spin multiplet are of primary interest, the effective spin Hamiltonian  $\hat{H}$  simply corresponds to the well-known giant-spin Hamiltonian  $\hat{H}_S$ . The effective spin operators  $\hat{S}_{j\beta}$  are then related to the components of the total spin operator  $\hat{S}_\beta$  via the projection coefficients  $\Gamma_1(i)$ , i.e.,  $\hat{S}_{i\alpha} = \Gamma_1(i) \hat{S}_\alpha$ .<sup>7</sup> The matrix elements of the local spin operators  $\hat{S}_{i\alpha}$  hence simply become

$$\langle n | \hat{S}_{i\alpha} | m \rangle = \Gamma_1(i) \langle \bar{n} | \hat{S}_\alpha | \bar{m} \rangle. \quad (7)$$

The eigenstates  $|\bar{n}\rangle$  are obtained from the diagonalization of the giant-spin Hamiltonian in the spin space  $|SM\rangle$ . The projection coefficients are determined as usual by<sup>5</sup>

$$\Gamma_1(i) = \frac{\langle \tau S | T^{(1)}(S_i) | \tau S \rangle}{\langle S | T^{(1)}(S) | S \rangle}, \quad (8)$$

where  $\langle \tau S | T^{(1)}(S_i) | \tau S \rangle$  is a reduced matrix element related to the eigenstate  $|\tau SM\rangle$  of the Heisenberg-exchange part  $\hat{H}_{ex}$  of the microscopic spin Hamiltonian, and  $\langle S | T^{(1)}(S) | S \rangle = \sqrt{(2S+1)S(S+1)}$  is the reduced matrix element in the spin space  $|SM\rangle$ .

A subtle point shall be mentioned here. The described procedure essentially correspond to the strong-exchange limit,<sup>5</sup> i.e., the first-order perturbational treatment of the magnetic anisotropy. However, the strong-exchange limit does not yield all relevant spin terms in the giant-spin Hamiltonian correctly, such as for instance the fourth-order terms, because it neglects a mixing of the spin multiplets.<sup>6,7,8,9</sup> In principle, a similar statement is also

true for the effective spin operators.<sup>7</sup> However, it turns out that the mixing of the spin multiplets has a small effect on the topography of the matrix elements  $\langle \bar{n} | \hat{S}_{i\alpha} | \bar{m} \rangle$  even for rather large magnetic anisotropy, such that the  $Q$  dependence of the INS intensity is very well reproduced in first order. This has been explicitly demonstrated in particular for the  $\text{Mn}_{12}$  cluster, see Fig. 3 of Ref. [7]. Therefore one finds that the local spin operators are related to the total spin operator via factors (the projection coefficients), which are determined completely by the Heisenberg interactions in the system.

Insertion of Eq. (7) into the INS formula (4), as appropriate for a single-crystal material, yields

$$I_{nm}(\mathbf{Q}) = \mathcal{F}(\mathbf{Q}) \sum_{\alpha\beta} (\delta_{\alpha\beta} - l_\alpha l_\beta) \text{Re} \left[ \langle \bar{n} | \hat{S}_\alpha | \bar{m} \rangle \langle \bar{m} | \hat{S}_\beta | \bar{n} \rangle \right] \quad (9)$$

with the interference factor

$$\mathcal{F}(\mathbf{Q}) = \sum_{ij} F_i(Q) F_j(Q) \cos(\mathbf{Q} \cdot \mathbf{R}_{ij}) \Gamma_1(i) \Gamma_1(j). \quad (10)$$

Because of the symmetry with respect to the interchange  $ij \rightarrow ji$ , the exponential is replaced by the cosine and the real part,  $\text{Re}[\cdot]$ , is introduced. It is interesting to note that the interference effects, described by  $\mathcal{F}(\mathbf{Q})$ , factorize.

For a powder sample, Eq. (7) should be inserted into, for instance, Eq. (6), which effectively replaces  $U_q^{(k)}(\tilde{\mathbf{S}}_i \tilde{\mathbf{S}}_j)$  by  $\Gamma_1(i) \Gamma_1(j) U_q^{(k)}(\tilde{\mathbf{S}} \tilde{\mathbf{S}})$ . The result is

$$I_{nm}(Q) = \sum_{kq} \mathcal{F}^{kq}(Q) U_q^{(k)}(\tilde{\mathbf{S}} \tilde{\mathbf{S}}) \quad (11)$$

with the interference factors

$$\mathcal{F}^{kq}(Q) = \sum_{ij} f_{ij}^{kq}(Q, \mathbf{R}_{ij}) \Gamma_1(i) \Gamma_1(j). \quad (12)$$

In contrast to the single-crystal case, where the interference factor depends on the orientation of the transferred momentum vector, here the interference factors depend only on its magnitude. There is an instructive relation between Eqs. (10) and (12), which is outlined in the Appendix.

The giant-spin approach has been often used to analyze INS data on SMMs.<sup>16,17</sup> However, as discussed in the introduction, it disregards the many-spin nature of the cluster; the interference factors are hence constants, and the predicted INS  $Q$  dependencies just flat. This fundamental deficiency is overcome by Eqs. (10) and (12), which reproduce  $Q$  dependencies accurately. They hence are much more preferable than the giant-spin approach. Importantly, for both the powder and single-crystal case the interference factors depend solely on the geometrical arrangement of the spin centers and the projection coefficients on each site. They do not depend, for instance, on the particular form of the giant-spin Hamiltonian. Hence, as the structure of the cluster is known, the measured  $Q$  dependencies provide direct information on the projection coefficients, and wherewith on the exchange-coupling constants. This is the basic idea of the present work, and Eqs. (10) and (12) are the explicit formulations of it.

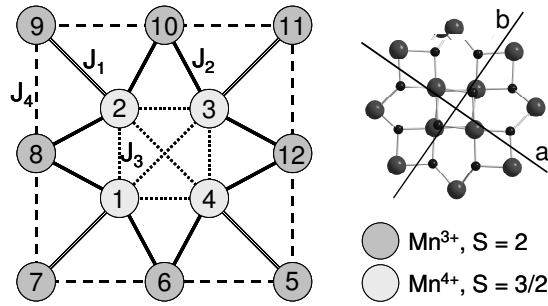


FIG. 1: Schematic representation of the spin centers and exchange-coupling paths in  $\text{Mn}_{12}$ . The spins 1-4 are denoted as core and the spins 5-12 as the crown. The right graphic shows the molecular structure of  $\text{Mn}_{12}$  viewed along the crystallographic  $c$  axis (only the Mn and the bridging oxygen atoms are shown). The orientations of the crystallographic  $a$  and  $b$  axes of the tetragonal unit cell are indicated. The core and crown are rotated with respect to the  $a$  and  $b$  axes such that the axis through spins 1 and 3 is rotated by  $12.33^\circ$  and that through spins 7 and 11 by  $10.91^\circ$ .

### III. PROJECTION COEFFICIENTS

As shown in the previous section, the evaluation of the INS  $Q$  dependence involves the geometrical structure of the cluster and the projection coefficients. The molecular structure of  $\text{Mn}_{12}$  is precisely known from x-ray crystallography ( $\text{Mn}_{12}$  crystallizes in space group  $I_4$  and exhibits a molecular  $S_4$  symmetry axis, see also Fig. 1).<sup>24</sup> In this section, the projection coefficients for  $\text{Mn}_{12}$  will be determined for various exchange-coupling topographies considered before in the literature.

The exchange-coupling graph appropriate for  $\text{Mn}_{12}$  is presented in Fig. 1. It involves the four exchange constants  $J_1$ ,  $J_2$ ,  $J_3$ , and  $J_4$ . Due to the  $S_4$  symmetry of the cluster, the projection coefficients assume three different values, namely

$$\Gamma_1(A) \equiv \Gamma_1(1) = \Gamma_1(2) = \Gamma_1(3) = \Gamma_1(4), \quad (13)$$

$$\Gamma_1(B) \equiv \Gamma_1(6) = \Gamma_1(8) = \Gamma_1(10) = \Gamma_1(12), \quad (14)$$

$$\Gamma_1(C) \equiv \Gamma_1(5) = \Gamma_1(7) = \Gamma_1(9) = \Gamma_1(11). \quad (15)$$

The indices  $A$ ,  $B$ , and  $C$  will be used also to notate the three sublattices consisting of the spins  $\{1, 2, 3, 4\}$ ,  $\{6, 8, 10, 12\}$ , and  $\{5, 7, 9, 11\}$ , respectively. Since  $\Gamma_1(A) + \Gamma_1(B) + \Gamma_1(C) = 1/4$  the projection coefficients are not independent of each other, and the  $Q$  dependence of the INS intensity is effectively governed by only two independent parameters.

The first idea on the coupling situation in  $\text{Mn}_{12}$  came from magneto-chemical considerations, which suggested that  $J_1$  is antiferromagnetic and much larger than the other three coupling constants.<sup>25</sup> Hence, the spins of e.g. the Mn ions 1 and 7 couple to an overall spin of  $1/2$ , and similar for the spins 2&9, 3&11, and 4&5. In order to arrive at a  $S = 10$  ground state, these spins are then coupled ferromagnetically to the remaining four Mn(III)

spins 6, 8, 10, and 12. Following Ref. [26], this scheme will be called the "Florentine" coupling scheme. Since the ground-state spin wavefunction is constructed here by a successive coupling of spins, the projection coefficients can be calculated easily using the Wigner-Eckart theorem and Racah formalism.<sup>5</sup>

A second scheme consists of coupling the eight Mn(III) spins ferromagnetically to yield an overall spin  $S_{BC} = 16$ , to couple the four Mn(IV) spins ferromagnetically to yield a spin  $S_A = 6$ , and then to couple these two spins antiferromagnetically to yield  $S = S_{BC} - S_A = 10$ .<sup>26</sup> This coupling scheme is based on the rationale that  $J_1$  and  $J_2$  are both antiferromagnetic, while  $J_3$  and  $J_4$  are assumed to be ferromagnetic. It will be called the "A+(B+C)" scheme. The projection coefficients again can be calculated easily using the Wigner-Eckart theorem and Racah formalism.

A third scheme consists of coupling the four spins of each sublattice  $A$ ,  $B$ ,  $C$  ferromagnetically, then to couple the spins of sublattices  $A$  and  $B$  antiferromagnetically to yield  $S_{AB} = 4$ , and to finally couple this spin with that of sublattice  $C$  antiferromagnetically to yield  $S = S_{AB} - S_C = 10$ . This coupling scheme is based on the rationale that  $J_1$  and  $J_2$  are both antiferromagnetic and dominating, such that the frustration induced by  $J_3$  and  $J_4$  is negligible. It will be called "(A+B)+C". The calculation of the projection coefficients proceeds as for the previous two schemes.

The above three schemes approximate the wavefunction of the ground-state spin multiplet by a spin wavefunction  $|\nu SM\rangle$ , where  $\nu$  denotes intermediate spin quantum numbers. The associated spin-coupling schemes were suggested by the different assumptions concerning the exchange-coupling topography. A more penetrating approach is of course to specify the values of the coupling constants  $J_1, \dots, J_4$  and to calculate the ground-state wavefunction numerically by exact diagonalization. Such an approach has been pursued for  $\text{Mn}_{12}$  by three groups. Raghu *et al.* suggested the set  $J_1 = -215$  K,  $J_2 = J_3 = -85$  K,  $J_4 = 64.5$  K.<sup>27</sup> The projection coefficients can be determined from the spin densities given in their work. Regnault *et al.* deduced the values  $J_1 = -119$  K,  $J_2 = -118$  K,  $J_3 = 8$  K,  $J_4 = -23$  K.<sup>28</sup> No information is given which would allow a determination of the projection coefficients. Hence we calculated them numerically using a sparse-matrix iterative subspace technique.<sup>7,29</sup> Finally, Chaboussant *et al.* deduced the values  $J_1 = -67.2$  K,  $J_2 = -61.8$  K,  $J_3 = -7.8$  K,  $J_4 = -5.6$  K.<sup>30,31</sup> Here too the projection coefficients were calculated by us numerically. The exchange-coupling constants were also evaluated by LDA+U and DFT calculations,<sup>32,33</sup> but these additional sets do not change the conclusions of this work and are hence not considered. The works Refs. [34,35,36], which start from an effective 8-spin model for  $\text{Mn}_{12}$ , are mentioned for completeness.

The projection coefficients of the six exchange-coupling topographies just described are compiled in Table I. For all cases,  $\Gamma_1(A)$  is negative while  $\Gamma_1(B)$  and  $\Gamma_1(C)$  are

TABLE I: Projection coefficients for the exchange-coupling topographies discussed in the text.

scheme	$\Gamma_1(A)$	$\Gamma_1(B)$	$\Gamma_1(C)$
Florentine	-0.05	0.2	0.1
A+(B+C)	-0.13636	0.19318	0.19318
(A+B)+C	-0.1	0.15	0.2
Raghu <i>et al.</i>	-0.09019	0.18103	0.15916
Regnault <i>et al.</i>	-0.12472	0.18376	0.19096
Chaboussant <i>et al.</i>	-0.12121	0.18398	0.18723

positive. This reflects the antiferromagnetic alignment of the spins of the Mn(IV) core with respect to the spins on the Mn(III) crown. The different exchange-coupling topographies clearly express themselves in different projection coefficients. However, the variation is not very pronounced, with the exception of the Florentine coupling scheme. For this scheme  $\Gamma_1(A)$  and  $\Gamma_1(C)$  are significantly smaller in magnitude, which reflects the assumption of a dominant  $J_1$  in this scheme.

#### IV. EXPERIMENTS

In the next sections, the  $Q$  dependence of the INS transition between the  $M = \pm 10$  and  $M = \pm 9$  levels of the  $S = 10$  ground-state multiplet of  $\text{Mn}_{12}$  will be considered. It occurs at an energy transfer of 1.24 meV, and is the strongest inelastic peak at liquid-He temperatures.

The best measurement so far of the  $Q$  dependence of this transition in powder samples of  $\text{Mn}_{12}$  has been reported by Hennion *et al.*<sup>20</sup> These authors studied a partially deuterated  $\text{Mn}_{12}$  sample on the triple-axis spectrometers 4F1 and 1T at the Laboratoire Leon Brillouin, Saclay, France, at a temperature of 1.55 K. The calculation of the  $Q$  dependence for powder  $\text{Mn}_{12}$ , which will be presented in the next section, hence will be compared to this data set.

In order to determine the  $Q$  dependence of a single-crystal sample, we performed measurements on an oriented array of about 500 non-deuterated single crystals of  $\text{Mn}_{12}$ . The crystals were synthesized following literature procedures.<sup>24</sup> The dimensions of the needle-shaped crystals were approximately  $5 \times 0.5 \times 0.5 \text{ mm}^3$ , and the masses ca. 2 mg.  $\text{Mn}_{12}$  crystallizes in the space group I4, hence the needle axis coincides with the magnetic anisotropy axis  $z$ . The oriented array of single crystals was obtained by placing crystals in long, narrow grooves milled into aluminium platelets, such that the needle ( $= z$ ) axes were aligned along the grooves.<sup>37</sup> A total of 15 such platelets which each held about 30–35 single crystals were stacked in an aluminium container and sealed therein. The INS intensity was measured on the time-of-flight spectrometer IN5 at the Institut Laue-Langevin, Grenoble, France. The initial neutron wavelength was set to 5.9 Å; the resolution at the elastic line was 60  $\mu\text{eV}$ . The sample was

inserted into an orange cryostat, permitting a sample temperature of 1.5 K. The data were corrected for the contribution of the sample container and the detector efficiency using a vanadium standard.

The alignment of the  $z$  axis of the quasi-single-crystal sample with respect to the transferred momentum vector  $\mathbf{Q}$  crucially influences the measured  $Q$  dependence. In simulations, details of the experiment have hence to be considered. The laboratory frame  $XYZ$  is chosen such that the  $X$  axis points along the wave vector of the incident horizontal neutrons,  $\mathbf{e}_X = \mathbf{k}/k$ , and the  $Z$  axis into the sky. In the experimental configuration of the IN5 spectrometer, the  $Y$  axis is then directed towards the side of the detector banks. The  $\mathbf{Q}$  vector lies in the  $XY$  scattering plane and is described by its magnitude  $Q$  and angle  $\varphi_Q$ ,  $\mathbf{Q} = Q(\cos \varphi_Q, \sin \varphi_Q, 0)$ , with  $Q_Y \leq 0$ . The calculation of matrix elements, however, is most conveniently done in the  $xyz$  frame of the molecular magnetic axes. As will be shown in the next section, the cluster can be treated as uniaxial, and the orientation of the sample hence described by the polar angles  $\theta$  and  $\varphi$  of its  $z$  axis in the  $XYZ$  frame. This procedure is not exactly correct, because the cluster coordinates are not invariant under rotations around  $z$ . We found, however, that this subtlety does not affect the conclusions of this work and hence do not exploit it further here. In our calculations the  $x, y$  axes were along the crystallographic  $a, b$  directions, see Fig. 1. The  $z$  axis in the  $XYZ$  frame is generated by two rotations,  $\mathbf{z} = R_Z(\varphi)R_Y(\theta)\mathbf{Z}$ . The transformation of a vector from the  $XYZ$  to the  $xyz$  frame is thus  $R_Y^{-1}(\theta)R_Z^{-1}(\varphi)$ , and for  $\mathbf{Q}$  in the  $xyz$  frame one obtains  $\mathbf{Q} = Q(\cos \theta \cos(\varphi_Q - \varphi), \sin(\varphi_Q - \varphi), \sin \theta \cos(\varphi_Q - \varphi))$ . The experimental data was taken for four different configurations, namely with the  $z$  axis along  $(0, 0, 1)$ ,  $(1, 0, 0)$ ,  $(0, 1, 0)$ , and  $(-1, 1, 0)$ , where  $(X, Y, Z)$  denotes a vector in the  $XYZ$  frame.

For comparison of experiment and calculation, it also has to be considered that the IN5 spectrometer measures the intensity as function of the direction  $\mathbf{k}'/k'$ , and not  $\mathbf{Q}$ . The data analysis software LAMP,<sup>39</sup> however, which was used for data reduction, yields the intensity as function of  $Q$  (which is related to  $\varphi_Q$  via the scattering triangle). Hence, the experimental  $Q$  dependencies include an implicit variation of  $\varphi_Q$ , i.e., the curves do not correspond to  $Q$  scans as they would be obtained on, e.g., triple-axis instruments.

#### V. $Q$ DEPENDENCE OF A POWDER SMM SAMPLE

In this section, the  $Q$  dependence of the  $M = \pm 10 \rightarrow \pm 9$  transition of a powder sample of  $\text{Mn}_{12}$  will be calculated for the six exchange topographies described in Sec. III, and compared to the experimental results of Hennion *et al.*<sup>20</sup> In order to proceed, the matrix elements  $\langle \bar{n} | \hat{S}_\alpha | \bar{m} \rangle$  have to be evaluated. Here  $|\bar{n}\rangle$  denotes one of the two states of the  $M = \pm 10$  level, and  $|\bar{m}\rangle$

one of the two states of the excited  $M = \pm 9$  level (the difference between  $|n\rangle$  and  $|\bar{n}\rangle$  is recalled, Sec. II).

Some points need clarification. First, a zero-field situation is considered. Hence, the wavefunctions may be chosen as real. The  $M = \pm 10$  and  $M = \pm 9$  levels each consist of two states, which shall be denoted as  $|0\rangle_{\pm}$  and  $|1\rangle_{\pm}$ , respectively. Since for these levels the tunnel splitting is way too small to be observed in INS, the intensity of the  $M = \pm 10 \rightarrow \pm 9$  transition in fact originates from four transitions. This is easily accounted for in the equations by considering each square of matrix elements to correspond to the sum  $\sum_{\mu\nu=\pm} \langle 0|_{\mu} \hat{S}_{\alpha} |1\rangle_{\nu} \langle 1|_{\nu} \hat{S}_{\beta} |0\rangle_{\mu}$ . Second, the eigenstates of the giant-spin Hamiltonian are not eigenstates of  $S_z$  because of the presence of terms such as  $B_{44} \hat{O}_4^{(4)}$ .<sup>11</sup> They hence cannot be labeled by  $M$  (we nevertheless use the notion of, e.g., a  $M = \pm 10$  level, its correct meaning should be obvious). The four lowest-lying states in fact are very well described by  $|0\rangle_{\pm} = (|10\rangle \pm |-10\rangle)/\sqrt{2}$  and  $|1\rangle_{\pm} = (|9\rangle \pm |-9\rangle)/\sqrt{2}$ . This means (i) that the matrix elements for the operator  $\hat{S}_z$  are essentially zero, and (ii) that the  $\text{Mn}_{12}$  molecule can be considered as magnetically uniaxial (in fact  $\sum_{\mu\nu=\pm} \langle 0|_{\mu} \hat{S}_{\alpha} |1\rangle_{\nu} \langle 1|_{\nu} \hat{S}_{\beta} |0\rangle_{\mu} = \sum_{M=\pm 10, M'=\pm 9} \langle M | \hat{S}_{\alpha} | M' \rangle \langle M' | \hat{S}_{\beta} | M \rangle$ ). These considerations are generally valid for the states of a SMM at the bottom of the energy barrier (in zero magnetic field).

With the choice of real wavefunctions,  $\langle \bar{n} | \hat{S}_z | \bar{m} \rangle = 0$ , and uniaxiality, only  $U_0^{(0)}$  and  $U_0^{(2)}$  in Eq. (6) are non-zero with  $U_0^{(2)} = -1/\sqrt{6} U_0^{(0)}$ . Hence one obtains

$$I_{nm}(Q) = \frac{2}{3} U_0^{(0)} \mathcal{F}_p(Q) \quad (16)$$

with the interference factor

$$\begin{aligned} \mathcal{F}_p(Q) = & \sum_{ij} F_i(Q) F_j(Q) \Gamma_1(i) \Gamma_1(j) \\ & \times [j_0(Q R_{ij}) - j_2(Q R_{ij}) \frac{3R_{ij,z}^2 - R_{ij}^2}{4R_{ij}^2}]. \end{aligned} \quad (17)$$

This is a rather general result. It holds for the INS transitions in a powdered SMM at the bottom of the energy barrier [it also implies that the  $Q$  dependence does not depend on  $M$ , only for states near the top of the barrier it may display deviations from  $\mathcal{F}_p(Q)$  due to the effects of  $\hat{S}_z$ ]. Interestingly, the interference factor again factorizes. The single-spin approach yields  $I_{nm}(Q) \propto U_0^{(0)}$ , i.e.,  $\mathcal{F}_p(Q) = \text{const.}$ <sup>7,16,17</sup> Comparison with Eq. (16) hence again nicely demonstrates the effect of the many-spin nature of a real spin cluster, which is expressed here by the interference factor  $\mathcal{F}_p(Q)$ .

The  $Q$  dependencies calculated from Eq. (17) are shown in Fig. 2(a) for the projection coefficients given in Table I. The form factors  $F_i(Q)$  were estimated with the standard analytical approximations.<sup>38</sup> The non-zero value for  $Q \rightarrow 0$  is typical for a  $\Delta S = 0$  transition.<sup>22</sup> After a steep drop with a minimum at about  $0.5 \text{ \AA}^{-1}$ ,

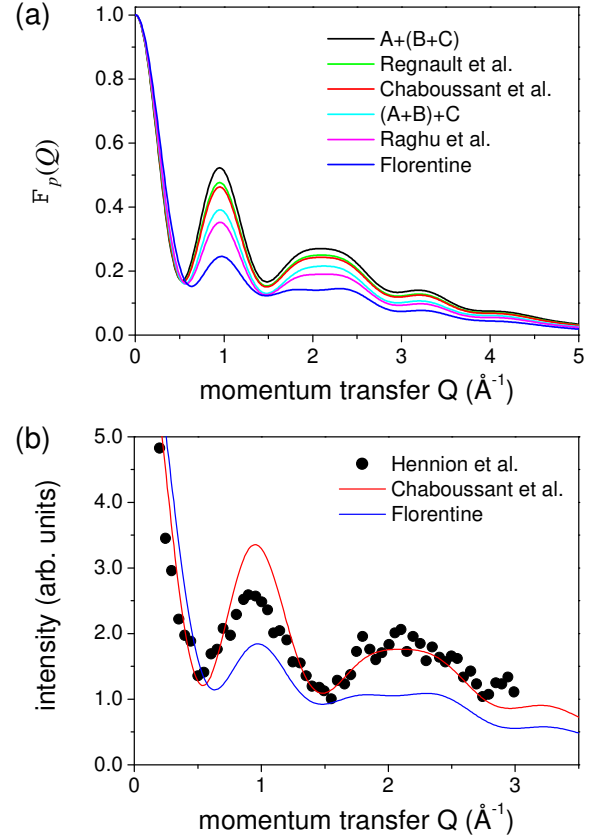


FIG. 2: (Color online) (a) Calculated  $Q$  dependencies of the intensity of the  $M = \pm 10 \rightarrow \pm 9$  transition in a powder sample of  $\text{Mn}_{12}$  for the six exchange-coupling topographies discussed in the text. Curves are labeled in the order of the height of the maximum at  $1 \text{ \AA}^{-1}$ . (b) Experimental data of Hennion *et al.* (reproduced from Ref. [20]). For comparison also the calculated curves for the Chaboussant *et al.* and Florentine coupling schemes are reproduced (the Chaboussant *et al.* curve was scaled such as to reproduce the data, the Florentine curve was then scaled by the same factor).

the curves exhibit a first pronounced maximum at about  $1.0 \text{ \AA}^{-1}$ , display a broad feature between ca.  $1.5$  and  $2.8 \text{ \AA}^{-1}$ , followed by further oscillations at higher  $Q$  values. Apparently, although significant variation is seen, the  $Q$  dependence of powder samples does not depend very sensitively on the exchange-coupling topography. The most significant effect is displayed by the height of the first maximum, which is most reasonably measured with respect to the two minima to the left and right. A qualitative comparison of Fig. 2(a) with Table I reveals that the height of the first maximum is correlated to the magnitude of  $\Gamma_1(A)$ . However, presumably it would require very precise experiments to measure this height reliably. The broad feature in the range  $1.5$ – $2.8 \text{ \AA}^{-1}$  looks very similar for all considered cases, with the exception of the Florentine coupling scheme, for which it exhibits two rather well resolved maxima at about  $1.8$  and  $2.4 \text{ \AA}^{-1}$ .

Figure 2(b) shows the experimental data from Ref. 20 for comparison. All calculated  $Q$  dependencies reproduce

the experimental curve more or less (the Chaboussant *et al.* curve has been also drawn as a representative for the five schemes other than the Florentine scheme, which all give similar agreement). The Florentine coupling scheme, however, shows the least agreement, see Fig. 2(b). First, the experimental height of the first maximum is clearly larger than calculated (in particular if one considers that e.g. incoherent scattering due to hydrogens should reduce the experimentally observed height). Second, the broad feature seems to be better reproduced by the other curves.

Hence, as a summary, the powder  $Q$  dependence shows some variation for different exchange-coupling topographies, but they are not easily differentiated in the experiment. However, it is fair to conclude that the Florentine coupling scheme is not consistent with the data, and can be ruled out (as has been found also before<sup>27,28,30,31</sup>). Hence, the powder  $Q$  dependence has some potential for differentiating between very different coupling topographies (it should be recalled that the Florentine scheme is distinguished from the others by its very dominant  $J_1$ ).

## VI. $Q$ DEPENDENCE OF A SINGLE-CRYSTAL SMM SAMPLE

In this section, the  $Q$  dependence of the  $M = \pm 10 \rightarrow \pm 9$  transition of a single-crystal sample of  $\text{Mn}_{12}$  will be considered. In this case, the INS intensity does not only depend on the magnitude of  $\mathbf{Q}$ , as in the powder case, but also on its orientation with respect to the sample. The orientation of  $\mathbf{Q}$  enters both Eqs. (9) and (10). Equation (9), however, can be further simplified. With real wavefunctions, the matrix elements of  $\hat{S}_x$  and  $\hat{S}_z$  are real, while those of  $\hat{S}_y$  are imaginary. Hence the sum over  $\alpha$ ,  $\beta$  reduces to

$$I_{nm}(\mathbf{Q}) = \mathcal{F}(\mathbf{Q}) \left[ \sum_{\alpha} (1 - l_{\alpha}^2) |\langle \bar{n} | \hat{S}_{\alpha} | \bar{m} \rangle|^2 - 2l_x l_z \times \langle \bar{n} | \hat{S}_x | \bar{m} \rangle \langle \bar{n} | \hat{S}_z | \bar{m} \rangle \right]. \quad (18)$$

Further considering that the matrix elements of  $\hat{S}_z$  are basically zero and that the cluster can be treated as magnetically uniaxial, as discussed in section V, one arrives at the approximation  $I_{nm}(\mathbf{Q}) = \mathcal{F}(\mathbf{Q}) (2 - l_x^2 - l_y^2) |\langle \bar{n} | \hat{S}_x | \bar{m} \rangle|^2$ .

Figure 3 shows the experimental results for the intensity of the  $M = \pm 10 \rightarrow \pm 9$  transition in our quasi-single-crystal sample of  $\text{Mn}_{12}$  for the four orientations with  $z$  parallel to  $(1,0,0)$ ,  $(-1,1,0)$ ,  $(0,1,0)$  and  $(0,0,1)$ , respectively (the vectors refer to the  $XYZ$  frame). Clearly, the  $Q$  dependence of the INS intensity depends very markedly on the orientation of the  $\mathbf{Q}$  vector with respect to the sample. The calculated  $Q$  dependencies are presented in Figure 4 for the six exchange-coupling topographies listed in Table I.

Comparison of Figs. 3 and 4 reveals that the experimental and theoretical curves exhibit very similar shapes

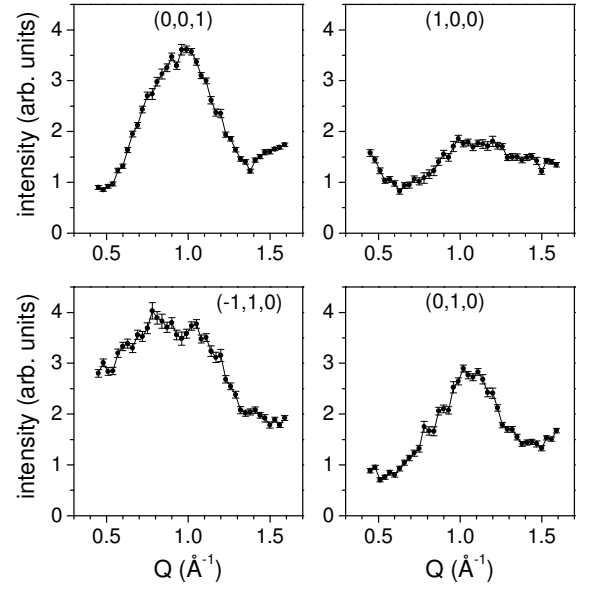


FIG. 3: Measured  $Q$  dependencies of the intensity of the  $M = \pm 10 \rightarrow \pm 9$  transition in a quasi-single-crystal sample of  $\text{Mn}_{12}$  for the four orientations of the  $z$  axis indicated in each panel. The normalization is arbitrary but identical for each curve; the curves hence correctly reflect relative intensities.

for each orientation. In particular, the positions of the minima and maxima are in good agreement. For the  $(0,0,1)$  direction, the experimental data shows a maximum at about  $0.95 \text{ \AA}^{-1}$ , which is embraced by two minima at about  $0.5$  and  $1.4 \text{ \AA}^{-1}$  with a slight upturn towards higher  $Q$ . In the  $(1,0,0)$  direction, the experiment exhibits a steep drop towards a minimum at about  $0.65 \text{ \AA}^{-1}$ , then a broad maximum at about  $1.2 \text{ \AA}^{-1}$  which is followed by a slow drop at higher  $Q$  values. The  $(-1,1,0)$  curve is characterized by a broad asymmetric feature with a maximum at about  $0.8 \text{ \AA}^{-1}$  and a steeper flank at the side of higher  $Q$  values. In the  $(0,1,0)$  direction, finally, the experiment shows a peak at about  $1.1 \text{ \AA}^{-1}$  with indications of two minima at about  $0.6$  and  $1.5 \text{ \AA}^{-1}$ . The theoretical curves reproduce these features very well.

However, also differences can be noted. In particular, the scattering intensities at the minima are significantly higher than predicted by theory. In fact, many of the minima are predicted to have almost zero intensity. This is not unexpected, it is a rather typical observation in non-deuterated samples and due to the large incoherent scattering of the hydrogen atoms.<sup>23,40,41</sup> Furthermore, while the relative intensities for the three directions  $(1,0,0)$ ,  $(-1,1,0)$ , and  $(0,1,0)$  are in accord with the theoretical trend, the  $(0,0,1)$  curve is almost a factor of 2 more intense than predicted. This could be an effect of the sample geometry, which is asymmetric in the sense that a neutron beam along the  $z$  axis has to traverse about  $1.5 \text{ cm}$  of  $\text{Mn}_{12}$  while a neutron beam in the  $xy$  plane traverses at most about  $0.8 \text{ cm}$ . This sug-



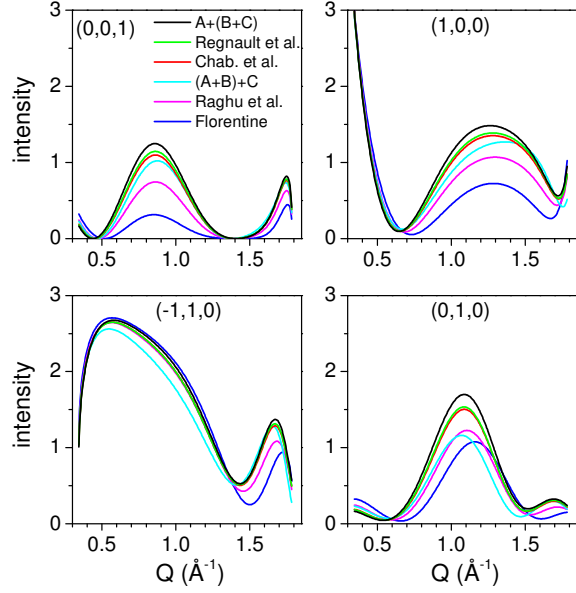


FIG. 4: (Color online) Calculated  $Q$  dependencies of the intensity of the  $M = \pm 10 \rightarrow \pm 9$  transition in a single crystal of  $\text{Mn}_{12}$  for the orientations of the  $z$  axis indicated in each panel. Each panel shows the results for the six exchange-coupling topographies listed in Table I.

gests that absorption is weaker in the  $(0,0,1)$  direction, consistent with the observation.

The theoretical curves in the  $(-1,1,0)$  and  $(0,1,0)$  directions are basically insensitive to the exchange-coupling topography, while for the height of the maximum in the  $(0,0,1)$  and  $(1,0,0)$  directions the same trend as found for the powder  $Q$  dependence, Fig. 2, is observed. Based on the very weak intensity expected for the Florentine coupling scheme, which is in contrast with the experiment, this scheme again is ruled out.

Besides the above conclusions we feel that the accuracy of the present experiment is not such as to allow further conclusions. At this point it is perfectly obvious to ask: how well can the projection coefficients be retrieved from the  $Q$  dependence and what would be an appropriate procedure. In order to explore this, the calculated INS intensity for the various exchange-coupling topographies for  $\text{Mn}_{12}$  is shown in Fig. 5 for the  $(0,0,1)$  direction as function of a momentum transfer in the  $XY$  plane [the  $(0,0,1)$  curves in the previous Fig. 4 correspond to cuts along the circle  $(Q_x - 1.065)^2 + Q_y^2 = (0.72)^2$ ]. Evidently, the single-crystal INS intensity exhibits features of significant intensity at certain special points, which are related to the molecular structure (*vide infra*). The intensity of these "towers", however, varies significantly with the exchange-coupling topography. A clear trend of the intensities is seen along the sequence  $A+(B+C)$ , Regnault *et al.*, Chaboussant *et al.*,  $(A+B)+C$ , Raghu *et al.*, and Florentine, which is the same trend noted before for the height of the maximum at about  $1 \text{ \AA}^{-1}$  [see Figs. 2(a) and 4].

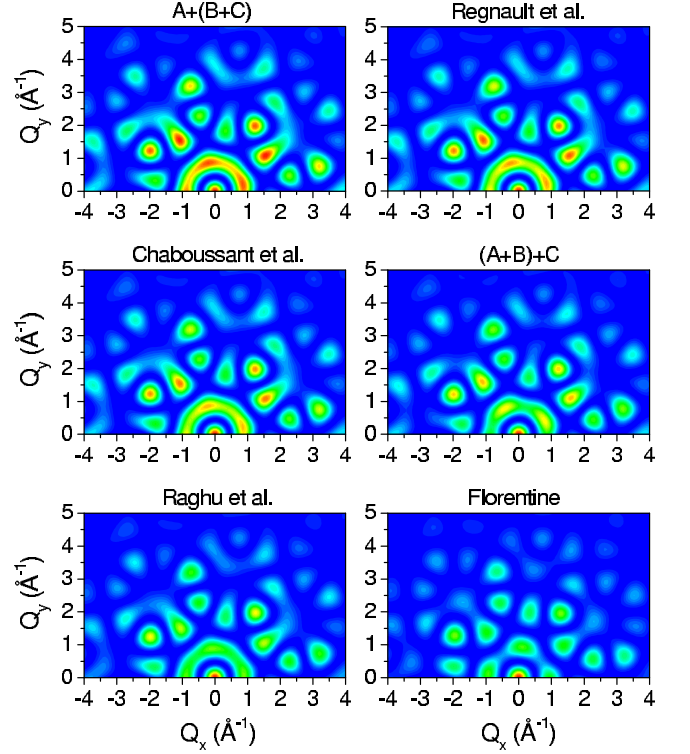


FIG. 5: (Color online) Calculated INS intensity of the  $M = \pm 10 \rightarrow \pm 9$  transition in a single crystal of  $\text{Mn}_{12}$  for the  $(0,0,1)$  orientation as function of the momentum transfer in  $x$  and  $y$  direction ( $Q_z = 0$ ). The INS intensity is represented by the color [dark gray (blue online) = 0, light gray (red online) = maximum]. Each panel shows the result for the indicated exchange-coupling topography.

A second, more striking trend can be observed. At  $Q \approx 1 \text{ \AA}^{-1}$  there is a circle of intensity, which exhibits four minima and maxima (if one goes around the full  $360^\circ$ ). While for the  $(A+B)+C$  scheme the left maximum (in the quadrant  $Q_y < 0$ ,  $Q_x > 0$ ) is at about  $-27^\circ$  from the  $y$  axis, it rotates to about  $+7^\circ$  in the sequence of  $(A+B)+C$ , Regnault *et al.*, Chaboussant *et al.*,  $A+(B+C)$ , Raghu *et al.*, and Florentine [the Florentine scheme in fact has its maxima where the  $(A+B)+C$  scheme has its minima, and vice versa]. Observation of the locations of the minima and maxima on the  $1 \text{ \AA}^{-1}$  circle would be hence very interesting.

A qualitative understanding of the intensity pattern can be obtained if one disregards the  $Q$  dependence of the form factors  $F_i(Q)$ , i.e., assumes  $F_i(Q) = 1$ . The  $\cos(\mathbf{Q} \cdot \mathbf{R}_{ij})$  factors in  $\mathcal{F}(\mathbf{Q})$ , Eq. (10), can be identically replaced by  $e^{i\mathbf{Q} \cdot \mathbf{R}_{ij}}$  [the same sum but with  $\sin(\mathbf{Q} \cdot \mathbf{R}_{ij})$  equals zero]. Then one finds

$$\mathcal{F}(\mathbf{Q}) = \int d\mathbf{R} e^{i\mathbf{Q} \cdot \mathbf{R}} \mathcal{G}(\mathbf{R}), \quad (19)$$

$$\mathcal{G}(\mathbf{R}) = \sum_{ij} \Gamma_1(i) \Gamma_1(j) \delta(\mathbf{R} - \mathbf{R}_{ij}), \quad (20)$$

i.e.,  $\mathcal{F}(\mathbf{Q})$  is just the Fourier transform of  $\mathcal{G}(\mathbf{R})$ . It should



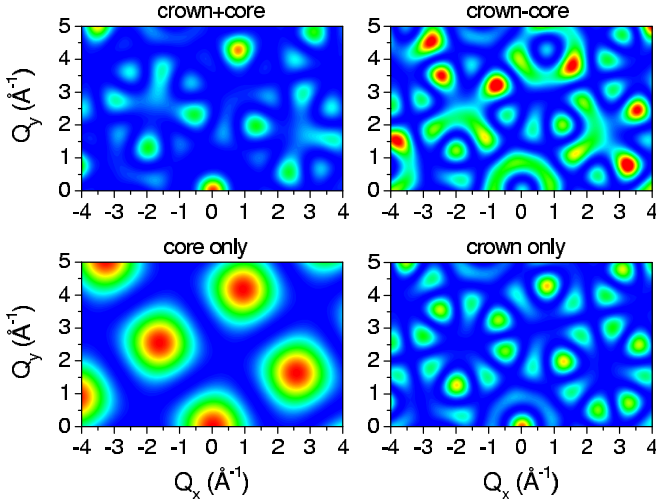


FIG. 6: (Color online)  $\mathcal{F}(\mathbf{Q})$ , Eq. (10), of  $\text{Mn}_{12}$  in the (0,0,1) orientation as function of the momentum transfer in  $x$  and  $y$  direction ( $Q_z = 0$ ). The value of  $\mathcal{F}(\mathbf{Q})$  is represented by the color [dark gray (blue online) = 0, light gray (red online) = maximum]. The panels show the results for the indicated situations discussed in the text.

be noted that the INS intensity  $I_{nm}(\mathbf{Q})$ , Eq. (9), in general cannot be Fourier transformed because of the  $\mathbf{Q}$  dependence of the sum. Exceptions are special cases such as uniaxial clusters with  $\mathbf{Q}$  in the  $xy$  plane. Then the sum is a constant, see also Eq. (18), and also  $I_{nm}(\mathbf{Q})$  is Fourier transformable [if  $F_i(Q) = 1$ ]. Since  $\mathcal{F}(\mathbf{Q})$  is the Fourier transform of the distance vectors  $\mathbf{R}_{ij}$  (and not of the position vectors  $\mathbf{R}_i$  as in diffraction), it exhibits maxima at  $\mathbf{Q} \cdot \mathbf{R}_{ij} \approx 2\pi n$ , which are, however, severely broadened since only a small number of metal centers is involved ( $n$  is an integer here).

It is revealing to plot  $\mathcal{F}(\mathbf{Q})$  for the cases  $\{\Gamma_1(A), \Gamma_1(B), \Gamma_1(C)\} = \{1, 1, 1\}$  ("crown+core"),  $\{-1, 1, 1\}$  ("crown-core"),  $\{0, 1, 1\}$  ("crown only"), and  $\{1, 0, 0\}$  ("core only"), as presented in Fig. 6. The crown+core case represents the direct Fourier transformation of the "density of distances"  $\sum_{ij} \delta(\mathbf{R} - \mathbf{R}_{ij})$  and mimics a fully ferromagnetic situation. The crown-core case in contrast mimics an antiferromagnetic alignment of the core spins with respect to the crown spins. The other two cases focus on the core and crown spins, respectively, i.e., neglect the interferences between core and crown.

The core-only plot demonstrates that indeed broadened peaks appear at  $\mathbf{Q} \cdot \mathbf{R}_{ij} \approx 2\pi n$  in  $\mathcal{F}(\mathbf{Q})$ . The comparison of the crown+core and crown-core plots shows that they are rather complementary in the sense that at the special  $\mathbf{Q}$  points the former has maximum intensity where the latter has minimum intensity, and vice versa. Most interestingly, the intensity circle at  $Q \approx 1 \text{ \AA}^{-1}$  is entirely absent in the crown+core plot while it is rather strong in the crown-core plot. It hence directly reflects the antiferromagnetic spin alignment of the core and

crown spins. The crown-only plot shows the contribution from the interference on the crown. It contributes only very weakly to the intensity at  $Q \approx 1 \text{ \AA}^{-1}$ .

This discussion shows that each feature visible in one of the plots of Fig. 5 can be related to certain pairs  $(i, j)$  of spin centers, and its amplitude to  $\Gamma_1(i)\Gamma_1(j)$ . One appropriate strategy to determine the values of  $\Gamma_1(i)\Gamma_1(j)$  would be thus to measure the INS intensity at the  $\mathbf{Q}$  points where  $\mathbf{Q} \cdot \mathbf{R}_{ij} = 2\pi n$ . Since most features appear for  $Q \gtrsim 2 \text{ \AA}^{-1}$ , it is now also obvious that the experiment presented in this section, which was limited to  $0.4 < Q < 1.6 \text{ \AA}^{-1}$ , could not be very successful in discriminating the different exchange-coupling topographies.

## VII. CONCLUSIONS

In this work the possibility of extracting the exchange-coupling constants of SMMs from the  $Q$  dependence of the INS intensity of transitions within the ground-state spin multiplet has been explored, with  $\text{Mn}_{12}$  as an example. The calculated  $Q$  dependence of powder SMM samples was found to show significant variations for different exchange-coupling situations, but in order to distinguish these experimentally, very precise measurements are required. The powder  $Q$  dependence has a potential to discriminate between very different exchange-coupling situations. In the case of  $\text{Mn}_{12}$ , the Florentine coupling scheme, which assumes a very dominating  $J_1$  interaction, could be discarded. The  $Q$  dependence of single-crystal SMM samples has a higher potential, because the additional dependence of the INS intensity on the orientation of the momentum transfer vector  $\mathbf{Q}$  allows for more independent measurements. The presented experimental results on a quasi-single-crystal  $\text{Mn}_{12}$  sample, which consisted of an oriented array of about 500 single crystals, however, did not allow us to infer information beyond that already concluded from the powder  $Q$  dependence. On the one hand, this is due to the obvious limitations of the experiments. On the other hand, a qualitative discussion of the situation shows that these experiments did not probe all the relevant  $Q$  space and indicates a better measurement procedure.

As a summary, deducing the exchange-coupling constants in SMMs from the INS  $Q$  dependence seems to be a viable strategy, but is experimentally challenging. It requires precise work in order to arrive at quantitative conclusions concerning the coupling constants. For instance, highly deuterated samples seem to be mandatory. Also, absorption corrections due to the actual sample geometry probably have to be employed, very much as in X-ray crystallography. However, although these issues clearly need further development, they are within reach of today's spectrometers.

The key point in the approach is the relationship between the exchange-coupling constants and the spin density map. For the SMMs it was noted in this work that

the spin density map can be determined from the  $Q$  dependence of the INS transitions within the spin ground state of the SMM. However, a similar approach is clearly also possible with other experimental techniques, which allow one to measure the spin density map, such as elastic neutron scattering or nuclear magnetic resonance.

### Acknowledgments

Financial support by the Swiss National Science Foundation and the European Union (EC-RTN-QUEMOLNA, Contract No. MRTN-CT-2003-504880) is gratefully acknowledged.

### APPENDIX A

In this Appendix, a relationship between the INS formulas for single-crystal and powder SMMs, i.e., Eqs. (9),(10) and (11),(12), respectively, shall be discussed. As mentioned already in Sec. VI, the interference factor  $\mathcal{F}(\mathbf{Q})$  of a single-crystal SMM, Eq. (10), can be written identically with  $\cos(\mathbf{Q} \cdot \mathbf{R}_{ij})$  replaced by  $e^{i\mathbf{Q} \cdot \mathbf{R}_{ij}}$ . Expanding the exponential in spherical harmonics,  $\mathcal{F}(\mathbf{Q})$  can be rewritten as

$$\mathcal{F}(\mathbf{Q}) = 4\pi \sum_{kq} (i)^k (-1)^q Y_q^{(k)}(\mathbf{Q}) C_k \mathcal{F}^{kq}(Q), \quad (\text{A1})$$

where

$$\mathcal{F}^{kq}(Q) = \sum_{ij} f^{kq}(Q, \mathbf{R}_{ij}) \Gamma_1(i) \Gamma_1(j), \quad (\text{A2})$$

$$f^{kq}(Q, \mathbf{R}_{ij}) = F_i(Q) F_j(Q) j_k(Q R_{ij}) T_q^{(k)}(\mathbf{R}_{ij}). \quad (\text{A3})$$

Here,  $k$  may be restricted to even values,  $k = 0, 2, 4, \dots$ .  $Y_q^{(k)}(\mathbf{V})$  denotes the  $q$ th component of the spherical harmonics of rank  $k$  related to the Cartesian vector  $\mathbf{V}$ . It is proportional to the irreducible spherical tensor  $T_q^{(k)}(\mathbf{V})$ ,  $Y_q^{(k)}(\mathbf{V}) = C_k T_q^{(k)}(\mathbf{V})$ , which also defines the proportionality constant  $C_{kq}$ .

This is the main finding of this Appendix: Equations (A2) and (A3) are identical to the results for the interference factors of powder SMM samples – if one expands  $I_{nm}(Q)$  in terms of the spherical tensors  $T_q^{(k)}$  and not the symmetrized spherical tensors  $U_q^{(k)}$  as in Eq. (11).

This point deserves comment. Equations (A3) and (12) look exactly identical, but in fact differ in the definition of the interference factors  $f^{kq}(Q, \mathbf{R}_{ij})$ : Equation (12) is derived from Eq. (6), which in turn is obtained by rewriting the general INS formula for powder samples, Eq. (5), in terms of the symmetrized spherical tensors  $U_q^{(k)}$ . Hence, the expressions for the  $f^{kq}(Q, \mathbf{R}_{ij})$  contain the tensors  $U_q^{(k)}(\mathbf{R}_{ij})$ .<sup>7</sup> An expansion in terms of  $U_q^{(k)}$  is most convenient for explicit calculations. The general powder formula Eq. (5), however, also can be expressed in terms of

the spherical tensors  $T_q^{(k)}$ . The resulting equations look exactly the same as that for  $U_q^{(k)}$ , but with all  $U_q^{(k)}$  replaced by  $T_q^{(k)}$  [for instance, replacing  $T_q^{(k)}$  by  $U_q^{(k)}$  in Eq. (A3) directly yields the equations (B2) of Ref. [7]]. In this Appendix, the  $T_q^{(k)}$ -expansion is preferred because the algebra is then more obvious, but in the expressions all  $T_q^{(k)}$  can be replaced identically by  $U_q^{(k)}$ . In this sense, Eqs. (A2) and (A3) are identical to the results for powder SMM samples, such that the above equations establish the sought-after relationship.

The relation Eq. (A1) is convenient. It separates the dependence of the INS intensity on the orientation of the  $\mathbf{Q}$  vector from the dependence on the magnitude  $Q$  and the cluster properties [which enter via  $\mathbf{R}_{ij}$  and  $\Gamma_1(i)$ ]. Furthermore, it establishes the connection between the single-crystal and powder interference factors (for the powder INS intensity, however, only the factors with  $k = 0, 2$  are relevant, while in the single-crystal case no such restriction exists).

Using the orthogonality relation for spherical harmonics, one obtains

$$\int \frac{d\Omega}{4\pi} \mathcal{F}(\mathbf{Q}) Y_q^{(k)}(\mathbf{Q}) = (i)^k C_k F^{kq}(Q). \quad (\text{A4})$$

Hence, integrating the interference factor  $\mathcal{F}(\mathbf{Q})$  over all orientations of  $\mathbf{Q}$  for a given magnitude  $Q$  allows one to extract the interference factors  $F^{kq}(Q)$ .

If one assumes  $F_i(Q) = 1$  for the moment, and uses the closure relation of spherical Bessel functions, one obtains

$$\int dQ Q^2 \mathcal{F}_q^{(k)}(Q) j_k(QR) = \frac{\pi}{2R^2} \sum_{ij} \Gamma_1(i) \Gamma_1(j) T_q^{(k)}(\mathbf{R}_{ij}) \delta(R - R_{ij}), \quad (\text{A5})$$

where  $R$  is an arbitrary number [the result also holds for the weaker condition of  $F_i(Q) = F(Q)$  for all  $i$  if  $\mathcal{F}^{kq}(Q)/F(Q)$  is considered instead of  $\mathcal{F}^{kq}(Q)$ ]. Hence, integrating  $\mathcal{F}^{kq}(Q)$  over  $Q$  using a value of  $R$  which matches one of the metal distances  $R_{ij}$  allows one to project out the value of  $\Gamma_1(i) \Gamma_1(j)$  for the pair  $(i, j)$  [to be precise, one has to assume that if  $R_{ij}$  is equivalent for several pairs  $(i, j)$  that then also  $\Gamma_1(i) \Gamma_1(j)$  is equivalent for these pairs, which is reasonable]. If one combines Eqs. (A4) and (A5) and sums over  $\sum_{kq} T_q^{(k)*}(\mathbf{R}_{ij})$ , then one recovers the Fourier transform of  $\mathcal{F}(\mathbf{Q})$ , Eq. (20).

A final comment: Obviously, very similar mathematics can be performed in order to establish relations between the INS formulas Eq. (4) and Eq. (6), which are valid for general spin clusters. Following the above lines, the corresponding equations are simple to obtain. They hence shall not be reproduced here.

- \* Corresponding author.  
E-mail: waldmann@iac.unibe.ch
- <sup>1</sup> R. Sessoli, D. Gatteschi, A. Caneschi, and M. A. Novak, *Nature (London)* **365**, 141 (1993).
  - <sup>2</sup> J. R. Friedman, M. P. Sarachik, J. Tejada, and R. Ziolo, *Phys. Rev. Lett.* **76**, 3830 (1996).
  - <sup>3</sup> L. Thomas, F. Lioni, R. Ballou, D. Gatteschi, R. Sessoli, and B. Barbara, *Nature (London)* **383**, 145 (1996).
  - <sup>4</sup> G. Christou, D. Gatteschi, D. N. Hendrickson, and R. Sessoli, *MRS Bull.* **25**, 66 (2000); D. Gatteschi and R. Sessoli, *Angew. Chem. Int. Ed.* **42**, 268 (2003).
  - <sup>5</sup> A. Bencini and D. Gatteschi, *Electron Paramagnetic Resonance of Exchange Coupled Clusters* (Springer, Berlin, 1990).
  - <sup>6</sup> E. Livioti, S. Carretta, and G. Amoretti, *J. Chem. Phys.* **117**, 3361 (2002).
  - <sup>7</sup> O. Waldmann and H. U. Güdel, *Phys. Rev. B* **72**, 094422 (2005).
  - <sup>8</sup> A. Wilson, J. Lawrence, E.-C. Yang, M. Nakano, D. N. Hendrickson, and S. Hill, *Phys. Rev. B* **74**, 140403 (2006).
  - <sup>9</sup> S. Accorsi, A.-L. Barra, A. Caneschi, G. Chastanet, A. Cornia, A. C. Fabretti, D. Gatteschi, C. Mortalo, E. Olivieri, F. Parenti, P. Rosa, R. Sessoli, L. Sorace, W. Wernsdorfer, L. Zobbi, *J. Am. Chem. Soc.* **128**, 4742 (2006).
  - <sup>10</sup> R. Bircher, G. Chaboussant, A. Sieber, H. U. Güdel, and H. Mutka, *Phys. Rev. B* **70**, 212413 (2004).
  - <sup>11</sup> Despite the tetragonal crystal structure of  $\text{Mn}_{12}$ , also a term  $E(\hat{S}_x^2 - \hat{S}_y^2)$  has been found to be significant, see e.g. Refs. [10,12,13,14]. This term affects strongly the tunneling splittings, but not the wave functions and anisotropy splitting of the states of relevance in this work. As the tunneling splittings are way too small to be detected in INS experiments, the actual terms responsible for tunneling can be disregarded for the purposes of this work.
  - <sup>12</sup> E. M. Chudnovsky and D. A. Garanin, *Phys. Rev. Lett.* **87**, 7203 (2001).
  - <sup>13</sup> S. Hill, R. S. Edwards, S. I. Jones, N. S. Dalal, and J. M. North, *Phys. Rev. Lett.* **90**, 217204 (2003).
  - <sup>14</sup> A. Cornia, R. Sessoli, L. Sorace, D. Gatteschi, A. L. Barra, and C. Daugebonne, *Phys. Rev. Lett.* **89**, 257201 (2002).
  - <sup>15</sup> K. W. H. Stevens, in *Magnetism*, edited by G. T. Rado and H. Suhl (Academic Press, New York, 1963), Vol. I.
  - <sup>16</sup> R. Caciuffo, G. Amoretti, A. Murani, R. Sessoli, A. Caneschi, and D. Gatteschi, *Phys. Rev. Lett.* **81**, 4744 (1998).
  - <sup>17</sup> I. Mirebeau, M. Hennion, H. Casalta, H. Andres, H. U. Güdel, A. V. Irodova, and A. Caneschi, *Phys. Rev. Lett.* **83**, 628 (1999).
  - <sup>18</sup> A. Furrer and H. U. Güdel, *Phys. Rev. Lett.* **39**, 657 (1977).
  - <sup>19</sup> O. Waldmann, *Phys. Rev. B* **68**, 174406 (2003).
  - <sup>20</sup> M. Hennion, L. Pardi, I. Mirebeau, E. Suard, R. Sessoli, and A. Caneschi, *Phys. Rev. B* **56**, 8819 (1997).
  - <sup>21</sup> A. Furrer and H. U. Güdel, *J. Magn. Magn. Mater.* **14**, 256 (1979).
  - <sup>22</sup> H. U. Güdel, in *Magneto-Structural Correlations in Exchange-Coupled Systems*, edited by R. D. Willet (Reidel, Amsterdam, 1985), p. 325.
  - <sup>23</sup> O. Waldmann, C. Dobe, H. U. Güdel, and H. Mutka, *Phys. Rev. B* **74**, 054429 (2006).
  - <sup>24</sup> T. Lis, *Acta Crystallogr., Sect. B* **35**, 2042 (1980).
  - <sup>25</sup> R. Sessoli, H.-L. Tsai, A. R. Schake, S. Wang, J. B. Vincent, K. Folting, D. Gatteschi, G. Christou, and D. N. Hendrickson, *J. Am. Chem. Soc.* **115**, 1804 (1993).
  - <sup>26</sup> F. Hartmann-Boutron, P. Politi, and J. Villain, *Int. J. Mod. Phys. B* **10**, 2577 (1996).
  - <sup>27</sup> C. Raghu, I. Rudra, D. Sen, and S. Ramasesha, *Phys. Rev. B* **64**, 064419 (2001).
  - <sup>28</sup> N. Regnault, Th. Jolicoeur, R. Sessoli, D. Gatteschi, and M. Verdaguer, *Phys. Rev. B* **66**, 054409 (2002).
  - <sup>29</sup> O. Waldmann, *Phys. Rev. B* **65**, 024424 (2002).
  - <sup>30</sup> G. Chaboussant, A. Sieber, S. Ochsenein, H.-U. Güdel, M. Murrie, A. Honecker, N. Fukushima, and B. Normand, *Phys. Rev. B* **70**, 104422 (2004).
  - <sup>31</sup> A. Honecker, N. Fukushima, B. Normand, G. Chaboussant, and H.-U. Güdel, *J. Magn. Magn. Matter.* **290**, 966 (2005).
  - <sup>32</sup> D. W. Boukhvalov, A. I. Lichtenstein, V. V. Dobrovitski, M. I. Katsnelson, B. N. Harmon, V. V. Mazurenko, and V. I. Anisimov, *Phys. Rev. B* **65**, 184435 (2002).
  - <sup>33</sup> K. Park, M. R. Pederson, and C. S. Hellberg, *Phys. Rev. B* **69**, 014416 (2004).
  - <sup>34</sup> M. I. Katsnelson, V. V. Dobrovitski, and B. N. Harmon, *Phys. Rev. B* **59**, 6919 (1999).
  - <sup>35</sup> A. K. Zvezdin and A. I. Popov, *Sov. Phys. JETP* **82**, 1140 (1996).
  - <sup>36</sup> I. Tupitsyn and B. Barbara, in *Magnetism: Molecules to Materials. Nanosized Magnetic Materials*, edited by J. S. Miller and M. Drillon (Wiley-VCH, Weinheim, 2002, p. 109).
  - <sup>37</sup> O. Waldmann, G. Carver, C. Dobe, D. Biner, A. Sieber, H. U. Güdel, H. Mutka, J. Ollivier, N. E. Chakov, *Appl. Phys. Lett.* **88**, 042507 (2006).
  - <sup>38</sup> P. J. Brown, in *Neutron Data Booklet*, edited by A. J. Dianoux and G. Lander (Institute Laue-Langevin, Grenoble, 2001).
  - <sup>39</sup> LAMP, the Large Array Manipulation Program. [http://www.ill.fr/data\\_treat/lamp/front.html](http://www.ill.fr/data_treat/lamp/front.html).
  - <sup>40</sup> T. Guidi, S. Carretta, P. Santini, E. Livioti, N. Magnani, C. Mondelli, O. Waldmann, L. K. Thompson, and L. Zhao, *Phys. Rev. B* **69**, 104432 (2004).
  - <sup>41</sup> O. Waldmann, C. Dobe, H. Mutka, A. Furrer, and H. U. Güdel, *Phys. Rev. Lett.* **95**, 057202 (2005).